



Primary production of light and s elements in very metal-poor Asymptotic Giant Branch stars

L. Husti¹, R. Gallino¹, S. Bisterzo¹, S. Cristallo², and O. Straniero²

¹ Dipartimento di Fisica Generale, Università di Torino, Via Pietro Giuria 1, 10125 Torino, Italy; e-mail: husti@ph.unito.it

² INAF - Osservatorio di Teramo (INAF), Teramo, Italy

Abstract. In AGB stars of low mass and very low metallicity, $[\text{Fe}/\text{H}] < -2$, a large abundance of primary ^{12}C obtained by partial He burning in the convective thermal pulse is mixed with the envelope by each third dredge up episode. A progressive amount of primary ^{22}Ne is produced in the He intershell by the conversion of all CNO nuclei to ^{14}N during H-burning shell, followed by double α capture in the thermal pulse. Despite its very low neutron cross section, ^{22}Ne contributes significantly to the production of primary ^{23}Na , ^{24}Mg , ^{25}Mg , ^{26}Mg . These last two are also obtained by α capture on ^{22}Ne . The neutron capture chain starting from ^{22}Ne continues up to iron, creating primary seeds for the s process. Further on, s elements are produced with high efficiency by neutron capture on the primary iron seeds. The third dredge up mixes with the envelope the freshly synthesized primary elements.

Key words. Stars: abundances – Stars: AGB – Stars: metal poor – Nucleosynthesis: light elements

1. Introduction

The AGB structure is characterized by a C-O core and by two alternate H and He burning shells. While the H burning shell progresses outwards, the region containing the ashes of H burning is heated up until He ignites quasi explosively, developing a thermal pulse (TP) that forces the whole region between the H shell and He shell (He intershell) to become convective. During the thermal pulse, a large abundance of ^{12}C is produced by partial He burning. At the quenching of the thermal pulse, the H shell is temporarily inactivated and the bottom of the convective envelope penetrates into

the top region of the He intershell, mixing with the surface freshly synthesized ^{12}C and s elements (third dredge up, TDU).

The major neutron source is the $^{13}\text{C}(\alpha, n)^{16}\text{O}$ reaction. During the third dredge up, where the H-rich convective envelope and the He-rich radiative zone get into contact, a small amount of protons is assumed to penetrate from the H-rich envelope into the top layers of the He intershell. At H reignition, these protons are captured by the large abundance of ^{12}C , giving rise to a ^{13}C pocket, via the reaction chain $^{12}\text{C}(\text{p}, \gamma)^{13}\text{N}(\beta^+ \nu)^{13}\text{C}$, eventually followed by $^{13}\text{C}(\text{p}, \gamma)^{14}\text{N}$ in case some extra protons survive the capture on the abundant ^{12}C . Later on, ^{13}C burns radiatively in the interpulse phase at $T \sim 0.9 \times 10^8$ K, thus

Send offprint requests to: L. Husti

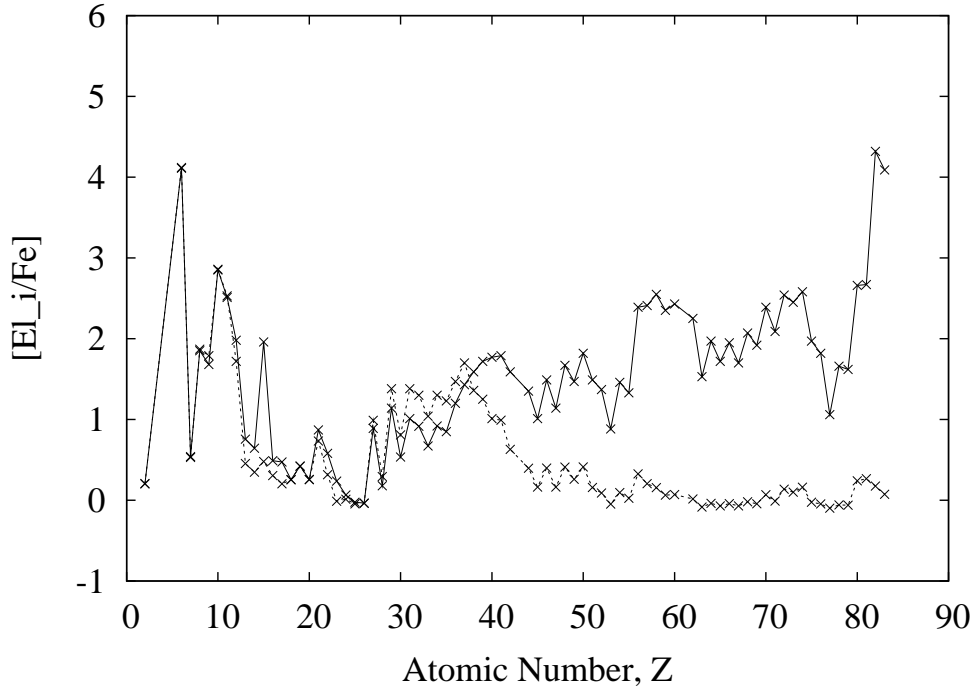


Fig. 1. Element abundance distributions for a $1.5M_{\odot}$ star, with $[\text{Fe}/\text{H}]=-2.6$. The solid line stands for the standard ST ^{13}C -pocket case, the dashed line stands for a case where neutrons are produced only by the ^{22}Ne (no ^{13}C -pocket).

releasing neutrons which are used for the build up of s-process elements. The s-rich pocket is then engulfed by the growing convective thermal instability. We consider a large range of ^{13}C pocket efficiencies, as required by the observations of s-enhanced stars at various metallicities (see Busso, Gallino & Wasserburg 1999; Bisterzo et al. 2005; Straniero, Gallino & Cristallo 2006). The ST case corresponds to a mass pocket of $9.37 \times 10^{-4} M_{\odot}$ containing a total mass of ^{13}C atoms of $4.69 \times 10^{-6} M_{\odot}$ distributed in three subzones. Starting from the top of the pocket, the masses of the three subzones are $7.5 \times 10^{-6} M_{\odot}$, $5.3 \times 10^{-4} M_{\odot}$, and $4.0 \times 10^{-4} M_{\odot}$; each subzone contains a mass fraction $X_{\text{eff}}(^{13}\text{C}) = 1.5 \times 10^{-2}$, 6.37×10^{-3} , and 3.0×10^{-3} , respectively. Here we consider *effective* ^{13}C mass fractions, defined as $X(^{13}\text{C}) - 13/14 X(^{14}\text{N})$. In fact, during the

subsequent release of neutrons by the reaction $^{13}\text{C}(\alpha, n)^{16}\text{O}$, any ^{14}N present in the zone would act as a major neutron poison via the resonant reaction $^{14}\text{N}(n, p)^{14}\text{C}$. For a general discussion of the choice of ^{13}C pocket and its profile we refer to Gallino et al. (1998). This ST case was used by Arlandini et al. (1999) and was shown to best reproduce the solar system main component with low mass AGB stellar models of half solar metallicity. Note that small variations in the choice of the ^{13}C pocket, including a finer subzoning, may provide essentially the same s-process distribution.

A second neutron source is provided by the $^{22}\text{Ne}(\alpha, n)^{25}\text{Mg}$ reaction, which is marginally activated during each convective thermal pulse. In very metal poor stars ($[\text{Fe}/\text{H}] < -2$), a large abundance of primary ^{12}C is mixed with the envelope by each third dredge up episode.

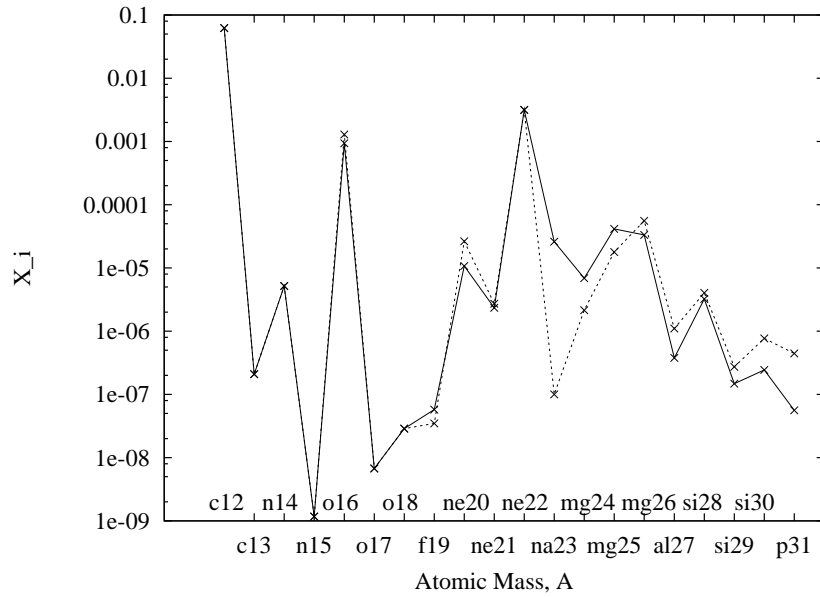


Fig. 2. Abundance distribution of light isotopes of a $1.5M_{\odot}$ star, with $[Fe/H]=-2.6$, when considering only ^{22}Ne neutron source. The solid line stands for the ordinary no ^{13}C -pocket case, the dashed line stands for the test case with no ^{13}C -pocket, in which the cross section of the $^{22}\text{Ne}(n,\gamma)^{23}\text{Ne}$ reaction is put to zero.

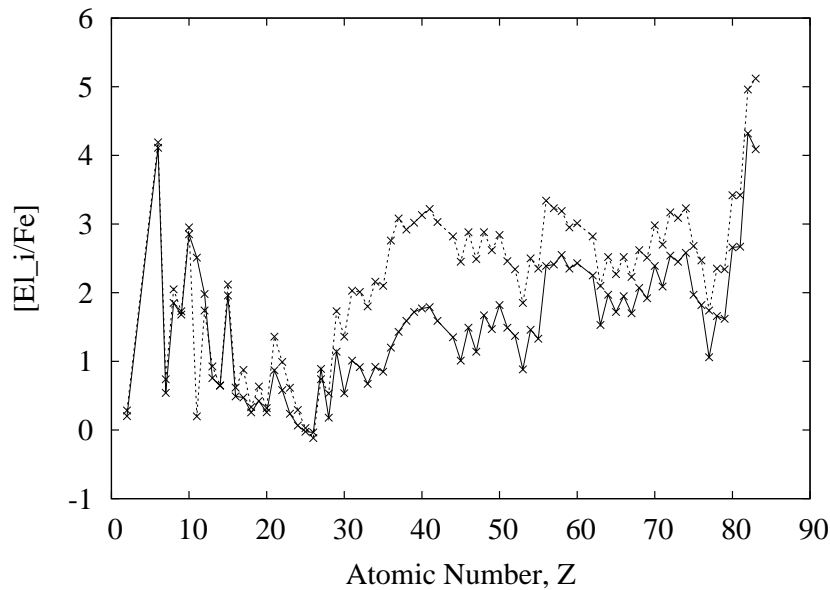


Fig. 3. Element abundance distributions for a $1.5M_{\odot}$ star, with $[Fe/H]=-2.6$. The solid line stands for the standard ST ^{13}C -pocket case, the dashed line stands for the test case with standard ST ^{13}C -pocket, in which the cross section of the $^{22}\text{Ne}(n,\gamma)^{23}\text{Ne}$ reaction is put to zero.

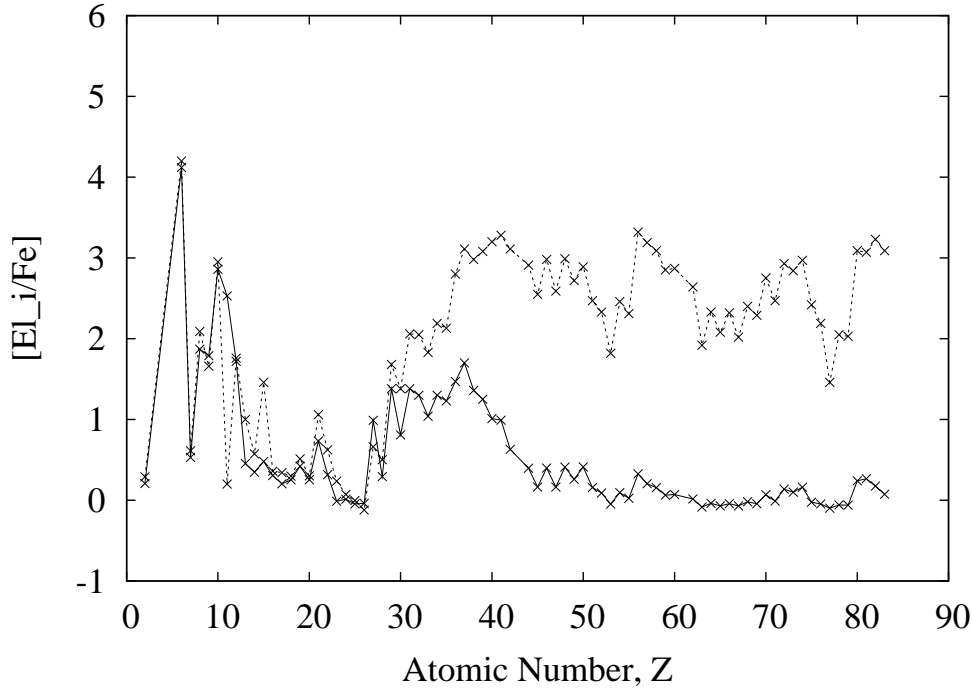


Fig. 4. Element abundance distributions for a $1.5M_{\odot}$ star, with $[\text{Fe}/\text{H}]=-2.6$. The solid line stands for the case with no contribution from ^{13}C as a neutron source (no ^{13}C -pocket), the dashed line stands for the test case with no ^{13}C -pocket, in which the $^{22}\text{Ne}(n,\gamma)^{23}\text{Ne}$ cross section is put to zero.

The subsequent activation of the H shell converts almost all CNO nuclei into ^{14}N . Thus the H burning ashes contain ^{14}N from the original CNO nuclei, plus an increasing amount of primary ^{14}N . During the subsequent convective thermal instability in the He shell, all the primary ^{14}N nuclides are converted to primary ^{22}Ne by the following reaction chain $^{14}\text{N}(\alpha,\gamma)^{18}\text{F}(\beta^+\gamma)^{18}\text{O}(\alpha,\gamma)^{22}\text{Ne}$. At the peak temperature reached at the base of the thermal pulse, the $^{22}\text{Ne}(\alpha,n)^{25}\text{Mg}$ reaction is partly activated, giving rise to a small neutron exposure.

2. Primary production of light elements

Although the neutron capture cross section of ^{22}Ne is very small ($\sigma(^{22}\text{Ne}, 30\text{keV})=0.059\pm 0.0057$ mbarn, Beer et al. 1991), at very low metallicities, the large

amount of primary ^{22}Ne acts as a major poison against the s process, significantly contributing to the production of primary light isotopes, such as ^{23}Na , ^{24}Mg , ^{25}Mg , ^{26}Mg . We note that neutron capture chain starting on ^{22}Ne gives rise not only to primary light elements, like Na and Mg, but to all the other elements up to iron, so that most of the iron seeds for the s-process are of primary origin. (see Gallino et al. 2006)

^{22}Ne acts as a neutron poison and meanwhile as a primary light element progenitor, both during the thermal pulse and during the interpulse phase, in the ^{13}C -pocket. In Fig. 1 we present the abundance distribution of a $1.5M_{\odot}$, $[\text{Fe}/\text{H}]=-2.6$ AGB model, when considering a standard ST ^{13}C -pocket and when considering only the ^{22}Ne neutron source. We see that there are no significant differences in the light element region, but the neutrons produced in

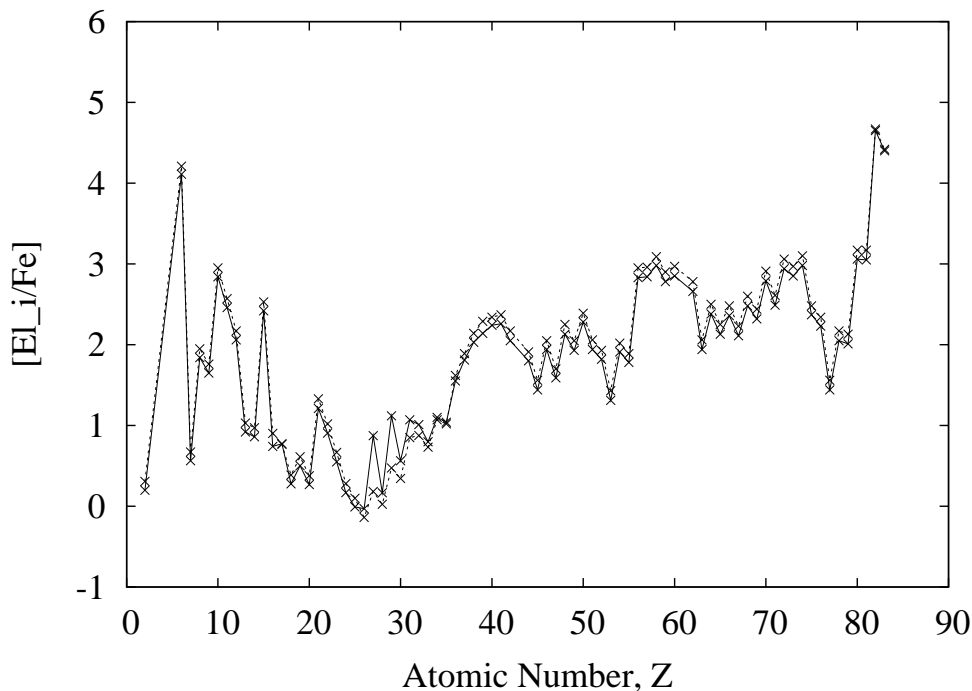


Fig. 5. Element abundance distributions for a $1.5M_{\odot}$ star, with $[Fe/H]=-2.6$. The solid line stands for the case with $ST \times 2$ ^{13}C -pocket, the dashed line stands for the test case with the same ^{13}C -pocket, in which the initial abundance of all isotopes from ^{56}Fe to ^{209}Bi put to zero.

the ^{13}C -pocket have an important contribution in the regions of the s elements, specially the heavy-s hs (from Ba to Nd) and lead.

In order to study the effect of neutron capture on ^{22}Ne and its consequences on the production of light elements, we put to zero the $^{22}Ne(n,\gamma)^{23}Ne$ cross section, in a test case. Fig. 2 shows an example of how the abundance distribution of light isotopes changes in the test case with respect to the ordinary case.

We notice that the envelope abundance of ^{23}Na decreases drastically, by a factor of 300 to 200, according to the strength of the ^{13}C -pocket, while the ^{22}Ne abundance remains unchanged. ^{24}Mg also decreases, by a factor of 3 to 5. Thus, the large primary production of ^{23}Na is a consequence of the neutron capture on primary ^{22}Ne . Also some primary production of ^{24}Mg derives from neutron captures on ^{23}Na . As ^{25}Mg and ^{26}Mg are also produced by

α capture on ^{22}Ne , the overall abundance of Mg is not significantly changed. As the cross section of $^{22}Ne(n,\gamma)^{23}Ne$ is put to zero, and Na is depleted drastically, a large abundance of neutrons survives, in the lack of these two major poisons, feeding the production of Al, Si and P, as well as the heavier elements.

3. Primary production of s elements

Neutron capture starting on primary ^{22}Ne is a very efficient process. In Fig. 4 we see that ^{22}Ne captures almost all the neutrons produced by itself through $^{22}Ne(\alpha,n)^{25}Mg$ reaction during the thermal pulse, but it also captures a lot of the neutrons produced by the ^{13}C -pocket (see Fig.3).

The neutron capture starting on primary ^{22}Ne produces an important amount of primary

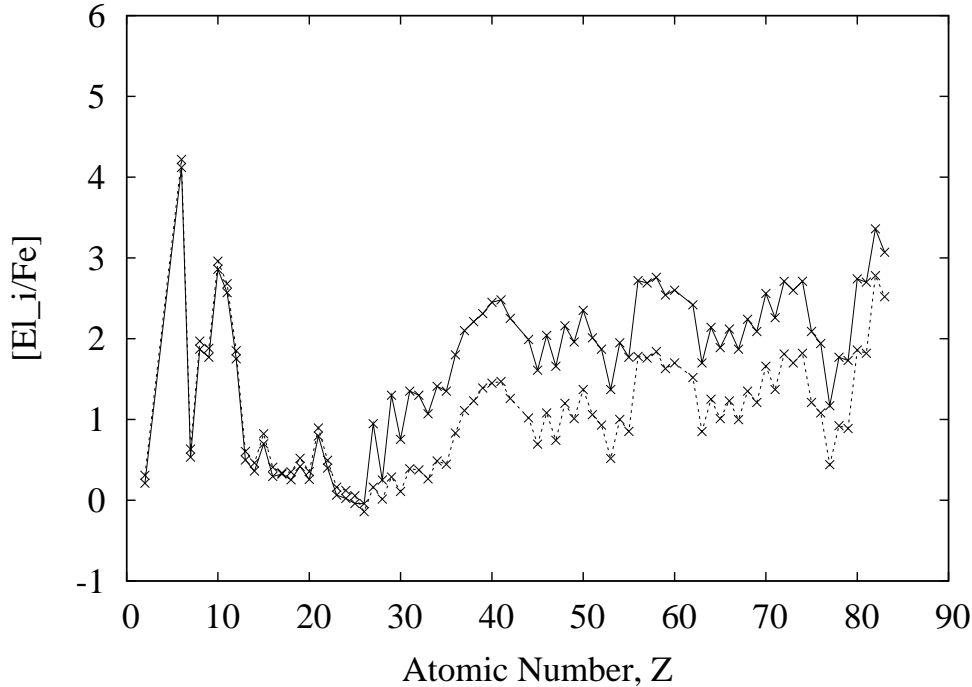


Fig. 6. Element abundance distributions for a $1.5M_{\odot}$ star, with $[\text{Fe}/\text{H}]=-2.6$. The solid line stands for the case with ST/2 ^{13}C -pocket, the dashed line stands for the test case with the same ^{13}C -pocket, in which the initial abundance of all isotopes from ^{56}Fe to ^{209}Bi put to zero.

iron which becomes the seed for the production of primary s-elements.

In a new test case we put to zero the initial abundances of all isotopes from ^{56}Fe up to ^{209}Bi (see Fig. 5). The primary s-element distribution depends on the efficiency of the ^{13}C -pocket. When neutrons are largely produced by the $^{13}\text{C}(\alpha, n)^{16}\text{O}$ reaction (ST $\times 2$ case), the initial abundance of the seed nuclei is unessential and a high percentage of the s elements is primary. If we consider a smaller ^{13}C -pocket, a lower amount of primary iron is produced, and as a consequence, the abundance of the primary s elements decreases (see Fig. 6). We note that primary iron is still produced even if we consider as neutron source only the $^{22}\text{Ne}(\alpha, n)^{25}\text{Mg}$ reaction, but in this case only the primary light-s elements are formed.

4. Conclusions

At very low metallicities, an important amount of ^{22}Ne is produced in a primary way. Although its cross section against neutron capture is very small, it acts as a strong neutron poison for the s-process and meanwhile a progenitor of primary light elements (specially Na) and primary iron seed for the s process. Neutron capture on the primary iron seeds produces primary s elements. The formation of primary iron and of primary s elements depends on the amount of available free neutrons, which are mainly produced by the ^{13}C -pocket.

References

- Arlandini, C., Käppeler, F., Wisshak, K., et al. 1999, *ApJ*, 525, 886
- Beer, H., Rupp, G., Voss, F., & Käppeler, F. 1991, *ApJ*, 379, 420

- Bisterzo, S., Gallino, R., Delaude, D., Straniero, O., & Ivans, I.I. 2005, in IAU Symp. 228, From Lithium to Uranium: Elemental Tracers of Early Cosmic Evolution, (ed. V. Hill, P. François, F. Primas), (Cambridge: Cambridge University Press), p. 481
- Busso, M., Gallino, R., & Wasserburg, G.J. 1999, *ARA&A* 37, 239
- Gallino, R., Arlandini, C., Busso, M., et al. 1998, *ApJ*, 497, 388
- Gallino, R., Bisterzo, S., Husti, L., Käppeler, F., Cristallo, S., & Straniero, O., 2006, POS(NIC-IX)100
- Straniero, O., Gallino, R., & Cristallo, S. 2006, *Nucl. Phys. A*, 777, 311